

# Impact of screening and relaxation onto weakly coupled 2D heterostructures

T.T. Nhung Nguyen<sup>1</sup>, T. Sollfrank<sup>1</sup>, and C. Tegenkamp<sup>1\*</sup>

<sup>1</sup> *Institut für Physik, Technische Universität Chemnitz,  
Reichenhainer Str. 70, 09126 Chemnitz, Germany*

E. Rauls<sup>2</sup> and U. Gerstmann<sup>3†</sup>

<sup>2</sup> *Department of Mathematics and Physics, University of Stavanger, Norway and*

<sup>3</sup> *Theoretische Materialphysik, Universität Paderborn, D 33098 Paderborn, Germany*

(Dated: May 18, 2021)

The stacking of different 2D materials provides a promising approach to realize new states of quantum matter. In this combined scanning tunneling microscopy (STM) and density functional theory (DFT) study we show that the structure in weakly bound, purely van der Waals (vdW) interacting systems is strongly influenced by screening and relaxation. We studied in detail the physisorption of lead phthalocyanine (PbPc) molecules on epitaxial monolayer graphene on SiC(0001) as well as on highly ordered pyrolytic graphite (HOPG), resembling truly 2D and anisotropic, semi-infinite 3D supports. Our analysis demonstrates that the different deformation ability of the vdW coupled systems, i.e. their actual thickness and buckling, triggers the molecular morphology and exhibits a proximity coupled band structure. It thus provides important implications for future 2D design concepts.

Heterostructures made layer by layer in a precisely chosen sequence out of 2D materials were suggested to design bulk quantum materials with entirely new functions [1]. Indeed, proximity coupling reveals superconductivity in twisted bilayer graphene [2, 3]. The absence of dangling bonds in 2D materials is expected to allow a flexible and lego-like epitaxial growth of lattice mismatched materials in random order [4].

However, as fabricating a 3D stack out of 2D sheets, the same layers may experience a different coupling, e.g. due to modified screening. Coulomb interaction in 2D and 3D is fundamentally different [5]. In contrast to the isotropic 3D case, for 2D the charge is redistributed on a circle around the point charge, i.e. the residual electric field depends on the polar angle, resulting in a non-local screening behavior which leads usually to strong and  $k$ -dependent renormalization of quasiparticle energies, e.g. excitons [6–8] and reduced energy gaps [9–11].

Among thousands of feasible 2D materials [12], graphene is still the most perfect and flexible one, thus ideal to elucidate principles of proximity coupling. Epitaxial graphene on SiC(0001) provides the flexibility to control the interface and its electronic properties [13–15]: monolayer graphene (MLG) grown on SiC(0001) is  $n$ -type doped while quasi-free monolayer graphene (QFMLG) on the same substrate is slightly  $p$ -type doped [16]. HOPG, in contrast, is charge neutral and represents the semi-infinite 3D counterpart of graphene [17].

Long-ranged ordered molecular 2D structures can be realized also by physisorption of  $\pi$ -conjugated organic molecules on surfaces [18]. Their combination with solid state 2D structures proposes advanced stacking sequences with tailored properties. However, the comprehensive understanding of the physisorption process can become a formidable challenge. Usually, the adsorbate

layer and surface lattice are not commensurate. Long-range dispersing forces between the molecules provide a possibility for various phases. The complex interaction scheme with the substrate often comes along with charge transfer (between substrate and adsorbate) superimposing the effect of screening.

Here, the shuttlecock-like lead phthalocyanine (PbPc) molecule with a large gap between the highest occupied and lowest unoccupied molecular orbitals, HOMO and LUMO, helps to suppress charge transfer with the substrate. It thus provides an excellent candidate to study implications of screening and proximity coupling in physisorbed systems. It contains four benzene-pyrrole moieties, which are connected via meso-aza nitrogens. The central Pb atom is coordinated to the four adjacent pyrrole nitrogens and is located outside the molecular plane further reducing the interaction with the substrate.

In this Letter, we analyzed the adsorption of PbPc on variously doped epitaxial graphene and HOPG. For QFMLG and MLG, the buckling of the graphene layer promotes a quasi-free, densely packed and chiral PbPc molecular layer structure with almost identical lattice parameters. Only minor 2D screening is observed, so that the molecular states remain almost unaffected. In contrast, large *substrate induced* dispersion of the HOMO is found on HOPG, where the more distant molecules interact via the substrate predominantly. Here,  $\pi$ -stacking leads to proximity coupling of PbPc with deeper graphite layers and to a strongly  $k$ -dependent reduction of the molecular gap.

As substrates epitaxial monolayer graphene (MLG) and hydrogen-intercalated quasi-free monolayer graphene (QFMLG) on semi-insulating 6H-SiC(0001) as well as highly ordered pyrolytic graphite (HOPG) were used. While HOPG resembles a charge neutral anisotropic 3D

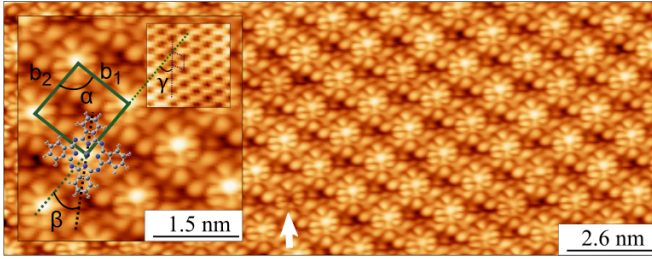


FIG. 1. Large scale STM image of a densely-packed molecular layer of PbPc on QFMLG (0.2 nA, +2 V). The imperfection (marked by an arrow) is most likely a Pc molecule with a missing Pb atom. The unit cell and relative orientation of the PbPc molecule w.r.t. graphene (small inset) are shown in the inset. The parameters are reported in Tab. I.

material, MLG and QFMLG are both 2D materials but with completely different electrochemical potentials [17]. Details about fabrication and characterization of the substrates are reported elsewhere [19–22]. The adsorption of PbPc molecules was done at 300 K under ultra high vacuum with same adsorption rates in order to allow a direct comparison [23]. The atomic structure and positions of molecular energy levels were investigated by low temperature scanning tunneling microscopy (LT-STM, 6 K and 80 K). Scanning tunneling spectroscopy (STS) was recorded using lock-in technique (20 meV, 1 kHz). For the  $dI/dV$  spectra an average of at least 10 curves were

TABLE I. Lattice parameters from STM and DFT for molecular PbPc layers on HOPG and (QF)MLG as well as for a freestanding PbPc layer.  $b_1$  and  $b_2$  denote the lattice constants as shown in Fig. 1.  $\alpha$ ,  $\beta$  and  $\gamma$  denote the angles of the unit cell, the rotation of the molecule and the orientation of the unit cell w.r.t. the graphene lattice, respectively. The minimum heights of adsorption  $d$  for atomic type (C/N/Pb) are indicated in Fig. 2, together with the tilting angle  $\vartheta$  of the molecules and the buckling  $\epsilon$  of the topmost C layer.  $N$  denotes the number of C atoms per layer.  $E_{b/C}$ ,  $E_{b/PbPc}$  and  $E_{b,intra}$  refer to the binding energies per substrate C atom, per molecule and the intra molecular layer contribution.

	free layer	MLG	QFMLG	HOPG
$b_1$ (nm)		$1.42 \pm 0.05$	$1.40 \pm 0.05$	$1.58 \pm 0.05$
calc.	1.35	1.37	1.37	1.54
$b_2$ (nm)		$1.38 \pm 0.05$	$1.40 \pm 0.05$	$1.49 \pm 0.05$
calc.	1.33	1.30	1.30	1.54
$\alpha$ ( $^\circ$ )		$90.3 \pm 1.0$	$90.0 \pm 1.0$	$90.1 \pm 1.0$
calc.	98.3	91.9	91.9	92.2
$\beta$ ( $^\circ$ )	—	$30 \pm 3$	$30 \pm 3$	$30 \pm 3$
$\gamma$ ( $^\circ$ )		$39.2 \pm 2.0$	$38.5 \pm 2.0$	$30.5 \pm 2.0$
calc.	—	39.4	39.1	30.0
height $d$ (Å)	—	2.5/3.5/4.6	2.3/3.5/4.7	3.1/3.3/4.7
buckling $\epsilon$ (Å)	—	0.51	0.67	0.02
tilting $\vartheta$ ( $^\circ$ )	—	9.2	9.5	0.2
$N_{C/layer}$	—	68	68	90
$E_{b/C}$ (meV)	—	29	31	26
$E_{b/PbPc}$ (eV)	1.18	1.97	2.11	2.35
$E_{b,intra}$ (eV)	1.18	0.25	0.24	0.01

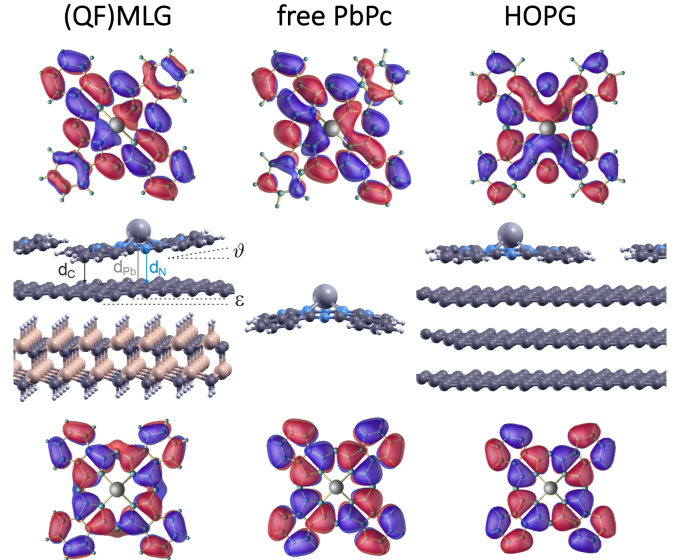


FIG. 2. Structure of PbPc monolayers on (QF)MLG (tilting angle  $\vartheta$ ) and HOPG, in comparison with isolated (free) PbPc molecules. The molecular HOMOs (bottom) and LUMOs (top) for the molecular species alone are also shown. For HOPG, the strong coupling to the other layers prevents the topmost layer from corrugation and buckling  $\epsilon$ , cf. Table I.

acquired at various positions across the molecules.

Our experiments are supplemented by DFT calculations using a supercell approach and periodic boundary conditions. For HOPG, molecular layers of PbPc molecules were modeled on 6 layer thick Bernal-stacked graphite. Thereby, the simplicity of the substrate allows a direct modeling in the experimentally observed quasi-square surface unit cell (with  $N=90$  atoms per C layer, see Tab. I). In contrast, for QFMLG and MLG, square unit cells are either incommensurable with the underlying SiC(0001) substrate or the graphene layers. As a result, the unit cell of PbPc on (QF)MLG/SiC(0001) contains at least two molecules. However, the absence of any indications in the STM experiment suggests that the SiC part of the substrate plays a minor role. Thus, the MLG calculations were restricted to a simplified unit cell containing one PbPc, where the interaction with the substrate (68 atoms per C layer) is reduced to the topmost graphene layer plus a partially H decorated buffer layer, whereby the level of doping increases almost linearly with the number of in this way  $sp^3$ -coordinated C atoms. The doping level, i.e. the position of the Dirac point  $E_D$  (cf. Fig. 5a), can thus be adjusted via the degree of H decoration. For a 0.4 eV shift determined experimentally [22], about 15 % of the C atoms of the buffer layer have to be covalently bound to the underlying SiC substrate (cf. Fig. 5b), in fair agreement with experiment [24].

Structural relaxation calculations are performed with the Quantum ESPRESSO package using periodic boundary conditions and a  $3 \times 3 \times 1$   $k$ -point sampling [25, 26]. STM images are simulated based on VASP calculations using

the Tersoff-Hamann approach to analyse the tunneling current [27]. Specifically, we use scalar relativistic norm-conserving pseudopotentials and a plane wave basis set with 90 Ry energy cutoff. For structure relaxation the semi-local PBE functional was used to include many-body effects due to exchange and correlation (XC). Afterwards the B3LYP hybrid functional was used to accurately determine the electronic structure for the PBE relaxed structures. The use of B3LYP closes the DFT-underestimation of the molecular HOMO-LUMO gap (see Ref. 28 and 29 and Table II), and allows a 1:1 comparison of the resulting density of states (DOS) with the experimental STS spectra. In all calculations the D3 dispersion correction was used for a reasonable description of non-local correlation effects [30].

Our experiments and calculations clearly reveal an adsorption of PbPc, where the central Pb atom is pointing upwards on HOPG as well as on epitaxial graphene, as shown in Fig. 1. At least 0.3 eV per molecule (0.72 eV on HOPG) is gained by this preferential adsorption geometry. This is in contrast to Au(111) surfaces, where PbPc molecules show both, up- and down configurations [31]. PbPc on Cu(100) and Ag(100) have been found to form a chiral monolayer structure, while on Pd(100) a stable *achiral* state was reported [32, 33]. The latter adsorption geometry was explained by stronger hybridization between the  $p_z$  orbital of the macrocyclic C atoms in PbPc and the  $4d$  orbitals of the Pd substrate.

PbPc on all the investigated graphene and graphite templates forms highly-ordered *chiral* monolayer structures with a single PbPc molecules in quasi-square unit cells, as shown in Fig. 1 exemplarily for QFMLG [23]. Table I summarizes the lattice parameters and molecular orientations which were deduced from STM images taken across the edges of the PbPc islands (cf. with Ref. [23]). They are nicely confirmed and rationalized by our DFT simulations, i.e. by minimizing total energy while varying cell size and shape.

The lattice parameters for PbPc on QFMLG and MLG are similar (even identical in theory), while the parameters found on HOPG are considerably larger by about 10% (cf. Tab. I). The different lattice parameters come along with specific details of the adsorption structure. The characteristic shuttlecock structure of the free PbPc relaxes upon physisorption on all the three substrates. In case of HOPG, the  $C_{4v}$  symmetry of the gas phase PbPc molecules is retained, but all wings are found almost planar, cf. Fig. 2. It maximizes the attractive vdW interaction *per molecule* with the graphene template and resembles the geometry of isolated physisorbed molecules [34–36]. The adsorption height of the C-atoms of about 3.1 Å (cf. Tab. I) is similar to the interlayer distance in graphite. Together with the planar adsorption geometry this suggests  $\pi - \pi^*$  stacking as a predominant driving force. In essence, this stacking gives rise to a proximity-

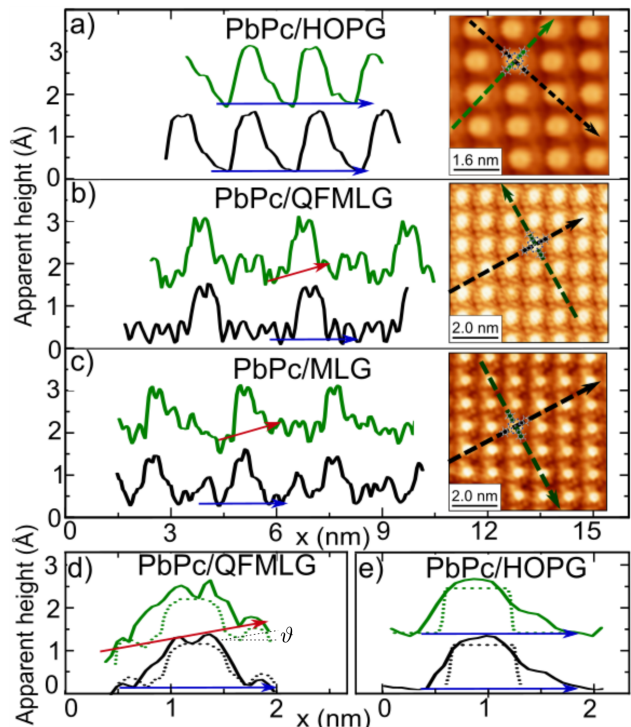


FIG. 3. High resolution STM images of PbPc monolayers on (a) HOPG (0.2 nA, -2 V), (b) QFMLG (0.2 nA, -2 V) and (c) MLG (0.2 nA, -1 V) and corresponding height profiles taken along two main molecular axes as indicated. A tilting (red arrows) is seen only on (QF)MLG along one direction (green). d) and e) show magnifications of PbPc/QFMLG and PbPc/HOPG, respectively, together with profiles (dotted lines) obtained from DFT calculated STM images, Fig. 4.

coupled band structure, as we will show below.

In contrast, the  $C_{4v}$  symmetry of the PbPc upon adsorption on (QF)MLG is lifted. Two neighboring benzene-pyrrole units are bended towards the surface, while the others are lifted to different extent (cf. Fig. 2). The formation of a layer of in this way tilted molecules is in agreement with the asymmetry seen in the STM height profiles taken along the two principal axes of the molecules on (QF)MLG (cf. Fig. 3 b,c). Details of the height profiles are shown in the close-up in panel d) and coincide in all cases with profiles obtained from DFT calculated STM images shown in Fig. 4.

The tilted structure on (QF)MLG allows a closer arrangement with strongly increased ( $\times 20$ ) intermolecular coupling,  $E_{b,intra}$  (see Tab. I) while providing a maximum binding energy *per substrate area* (i.e. per C-atom). The resulting lattice constants are about 10% smaller than on HOPG and, notably, comparable to a potential free-standing molecular PbPc layer [37].

*What is the driving force behind the different adsorption schemes?* — The geometry of PbPc on MLG and QFMLG is very similar, despite their different electrochemical potentials. Obviously, the doping level of the two 2D substrates are of minor relevance [17]. According



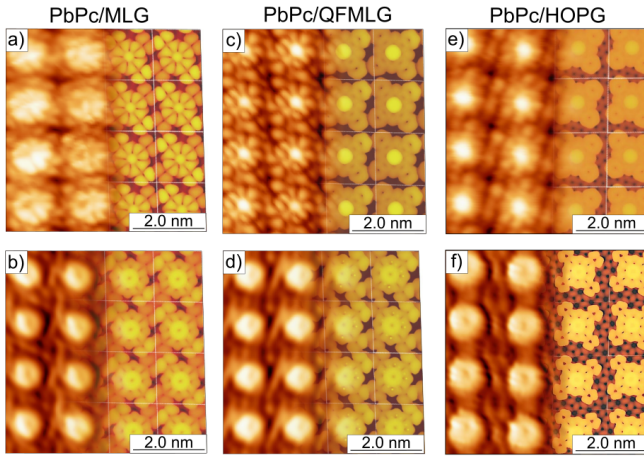


FIG. 4. Comparison of measured (left) and DFT simulated (right) STM patterns for negative (HOMO, bottom) and positive voltages (LUMO, top), i.e. occupied and empty states. The tunneling conditions, given in (nA/V), were: a) 0.2/+2, b) 0.2/-2, c) 0.2/+2, d) 0.5/-2, e) 0.1/+1.6, f) 0.2/-2, whereby the current was chosen in order to optimize the contrast.

to recent transport measurements [23], charge transfer is also not taking place, in agreement with the present STS and DFT calculations (see below).

A conceivable reason is the corrugation of epitaxial graphene on SiC. The buckling facilitates adsorption of *tilted* PbPc molecules: The topmost graphene layer is considerably upwards bended towards the PbPc macrocycle compensating the tilting-induced losses in vdW interaction. Although the exfoliation energy for HOPG is one order of magnitude lower than in case of MLG/SiC [38, 39] a local deformation of the uppermost C layer in HOPG costs by far more energy (182 meV instead of 86 meV for MLG). Obviously, the inherent corrugation of epitaxial graphene layers (the lateral strain also responsible for the buckling) allows for a flexible adaption of the substrate to the adsorbed molecular structures. Thus, the tilting of the PbPc molecule is a direct consequence of the deformation ability of the 2D support. A common STM feature for all three substrates is a donut-like shape of the occupied state in the center of the molecule. It was seen for all investigated substrates and is nicely reproduced by DFT in Fig. 4 [23]. This demonstrates that the central Pb atom does not contribute to the HOMO (cf. Fig. 2, 5b,c) for all investigated substrates, whereby this spectroscopic fingerprint becomes most obvious at slightly different tunneling voltages, see Fig. 4. For a more detailed analysis, additional STS measurements were performed. In Fig. 5 a) averaged  $dI/dV$ -spectra are shown and compared with the B3LYP-D3 calculated density of states (DOS):

(i) While the energies for the HOMO and LUMO states of gas phase PbPc [28] and adsorbed on QFMLG as well as HOPG are similar, the spectrum measured on MLG is shifted to lower energies (by  $\approx 0.4$  eV), reflect-

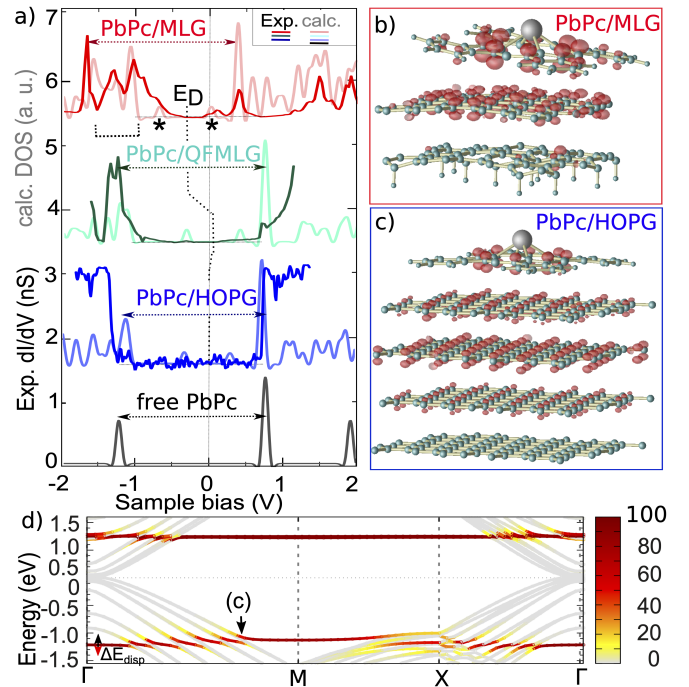


FIG. 5. a) Averaged  $dI/dV$  spectra (set-point: 0.2 nA, -1 V) taken for PbPc on MLG, QFMLG and HOPG compared with calculated DOS (B3LYP-D3, shifted  $3 \times 3 \times 3$   $k$ -sampling). Structure and molecular HOMO interacting with the substrate for MLG (b) and HOPG (c), whereby the spatial distribution of the HOMO (red) is exemplarily shown for a  $k$ -point indicated by the arrow in d): For HOPG, the  $k$ -dependent contributions of the molecule (in %) to the HOMO and LUMO are indicated by the color scale (d). The  $\pi$ -states of the substrates are labeled by (\*). Due to finite  $k$ -sampling, they appear at finite energies (centered around the Dirac point  $E_D$ ).

ing the  $n$ -type doping of MLG. Whereas the position of the LUMO is obvious also in this case, the identification of the HOMO requires theoretical support: Those C atoms (of the buffer layer) covalently bound to the SiC substrate, introduce additional occupied states partially superimposing the HOMO (see bracket in Fig. 5).

(ii) Interestingly, the different doping levels of MLG and QFMLG play no role. Very similar HOMO and only slightly different LUMO STM signatures suggest that both structures experience an almost identical lateral screening behavior. There are also only minor relative shifts of the HOMO and LUMO levels (cf. Tab. II). This is in line with literature where relevant screening effects onto the molecular electronic structure are restricted to substrate 2D-layer distances clearly below  $3 \text{ \AA}$  [40, 41]. Contrary, for HOPG our B3LYP-D3 band structure calculations reveal a large dispersion of the molecular HOMO ( $\Delta E_{disp} \approx 0.39$  eV). The LUMO is affected by much lower extend (cf. Fig. 5 d). Similar to the case of metallic substrates [33, 34], the resulting  $k$ -point dependent renormalization of the molecular HOMO-LUMO



gap can be attributed to  $\pi$ -stacking of the eight macrocyclic C atoms (those bridging two N atoms) with the substrate C atoms (see Fig. 5 b,c) which is largest for the second graphite layer. Notably, this hybridization effect is not coming along with a gap opening in the substrate bands and, thus, mimics an example of proximity coupling. The concomitant modification of the band structure is strongly  $k$ -dependent, and the maximum size effect is restricted to rather small regions within the Brillouin zone (Fig. 5 d), explaining the shoulder observed in STS slightly below  $-1$  V sample bias. The fact, that the molecular states of PbPc on HOPG reveal a strongly enhanced dispersion, although the intermolecular distance is larger compared to (QF)MLG, underlines the importance of a substrate mediated interaction.

In summary, we comprehensively studied vdW interacting heterostructures by means of PbPc monolayer structures on 2D graphene, (QF)MLG, and semi-infinite 3D graphite, HOPG. Albeit the surface structure of all templates are the same and charge transfer is not taking place, the molecular layer reveals very different lattice parameters and underwent different relaxation schemes. Formation of almost identical densely packed PbPc molecular layers with strongly tilted molecules were found on both 2D templates, despite their very different work functions, showing that lateral Thomas Fermi screening plays a minor role. Contrary, the interaction with the upper graphite (HOPG) layers, *in particular the second*, favors an almost planar adsorption of PbPc at the expense of a considerably larger lattice constant. The dispersing molecular states unambiguously demonstrate the presence of a substrate mediated interaction and the band structure exhibits spectral features of proximity coupling. Therefore, the actual thickness of a 3D stack built from 2D sheets appears to be decisive for the vdW heteroepitaxy and impacts recent layer by layer de-

TABLE II. Calculated HOMO-LUMO gap energies (eV, B3LYP-D3 hybrid functional) for PbPc on various substrates. For comparison the values for isolated (single) molecules (also for (semi-)local PBE/LDA functionals) and freestanding molecular monolayers (B3LYP-D3) are also given. For the periodic structures the  $k$ -point dependence ( $12 \times 12 \times 1$  sampling) is documented by the minimum/maximum values and the dispersion  $\Delta E_{\text{disp}} = \text{gap}_{\text{max}} - \text{gap}_{\text{min}}$ .

System (XC-funct.)	isolated	$\text{gap}_{\text{max/min}}$	$\Delta E_{\text{disp}}$
PbPc isolated (LDA,PZ-D3)	1.32		
PbPc isolated (PBE-D3)	1.33		
PbPc isolated (B3LYP-D3)	2.01		
freestanding PbPc film (MLG)	2.03/2.00		0.03
freestanding PbPc film (QFMLG)	2.01/2.00		0.01
freestanding PbPc film (HOPG)	2.01/2.01		0.00
PbPc/MLG	1.98	1.98/1.94	0.05
PbPc/QFMLG	1.95	1.94/1.85	0.09
PbPc/HOPG	2.00	2.00/1.75	0.39

sign concepts [1, 4].

### Acknowledgement

We thank D. Momeni Pakdehi (PTB Braunschweig) for providing us epitaxially grown graphene samples on SiC(0001). Financial support by the DFG (through project Te386/17-1 and TRR 142, project number 231447078) is gratefully acknowledged. The in parts demanding numerical calculations were possible thanks to CPU-time grants of the Paderborn Center for Parallel Computing, (PC)<sup>2</sup>.

\* christoph.tegenkamp@physik.tu-chemnitz.de

† uwe.gerstmann@upb.de

- [1] A. K. Geim and I. V. Grigorieva, *Nature* **499**, 419 (2013).
- [2] K. S. Novoselov, D. V. Andreeva, W. Ren, and G. Shan, *Frontiers of Physics* **14**, 13301 (2019).
- [3] Y. Cao, V. Fatemi, S. Fang, K. Watanabe, T. Taniguchi, E. Kaxiras, and P. Jarillo-Herrero, *Nature* **556**, 43 (2018).
- [4] A. Koma, *Journal of Crystal Growth* **201-202**, 236 (1999).
- [5] P. Cudazzo, I. V. Tokatly, and A. Rubio, *Phys. Rev. B* **84**, 085406 (2011).
- [6] D. Y. Qiu, F. H. da Jornada, and S. G. Louie, *Phys. Rev. Lett.* **111**, 216805 (2013).
- [7] M. M. Ugeda, A. J. Bradley, S.-F. Shi, F. H. da Jornada, Y. Zhang, D. Y. Qiu, W. Ruan, S.-K. Mo, Z. Hussain, Z.-X. Shen, F. Wang, S. G. Louie, and M. F. Crommie, *Nature Materials* **13**, 1091 (2014).
- [8] D. Y. Qiu, F. H. da Jornada, and S. G. Louie, *Nano Lett.* **17**, 4706 (2017).
- [9] J. B. Neaton, M. S. Hybertsen, and S. G. Louie, *Phys. Rev. Lett.* **97**, 216405 (2006).
- [10] J. M. Garcia-Lastra, C. Rostgaard, A. Rubio, and K. S. Thygesen, *Phys. Rev. B* **80**, 245427 (2009).
- [11] K. Noori, N. L. Q. Cheng, F. Xuan, and S. Y. Quek, *2D Materials* **6**, 035036 (2019).
- [12] N. Mounet, M. Gibertini, P. Schwaller, D. Campi, A. Merkys, A. Marrazzo, T. Sohier, I. E. Castelli, A. Cappelletti, G. Pizzi, and N. Marzari, *Nature Nanotechnology* **13**, 246 (2018).
- [13] C. Riedl, C. Coletti, and U. Starke, *Journal of Physics D: Applied Physics* **43**, 374009 (2010).
- [14] G. R. Yazdi, T. Iakimov, and R. Yakimova, *Crystals* **6**, 53 (2016).
- [15] M. Kruskopf, D. M. Pakdehi, K. Pierz, S. Wundrack, R. Stosch, T. Dziomba, M. Götz, J. Baringhaus, J. Aprozjan, C. Tegenkamp, J. Lidzba, T. Seyller, F. Hohls, F. J. Ahlers, and H. W. Schumacher, *2D Materials* **3**, 041002 (2016).
- [16] C. Riedl, C. Coletti, T. Iwasaki, A. A. Zakharov, and U. Starke, *Phys. Rev. Lett.* **103**, 246804 (2009).
- [17] S. Mammadov, J. Ristein, J. Krone, C. Raidel, M. Wanke, V. Wiesmann, F. Speck, and T. Seyller, *2D Materials* **4**, 015043 (2017).
- [18] J. M. Gottfried, *Surface Science Reports* **70**, 259 (2015).
- [19] C. Riedl, A. A. Zakharov, and U. Starke, *Applied Physics Letters* **93**, 033106 (2008).
- [20] C. Riedl, C. Coletti, T. Iwasaki, A. A. Zakharov, and

- U. Starke, *Phys. Rev. Lett.* **103**, 246804 (2009).
- [21] D. Momeni Pakdehi, J. Aprojanz, A. Sinterhauf, K. Pierz, M. Kruskopf, P. Willke, J. Baringhaus, J. P. Stöckmann, G. A. Traeger, F. Hohls, C. Tegenkamp, M. Wenderoth, F. J. Ahlers, and H. W. Schumacher, *ACS Applied Materials & Interfaces* **10**, 6039 (2018), PMID: 29377673.
- [22] D. Momeni Pakdehi, K. Pierz, S. Wundrack, J. Aprojanz, T. T. N. Nguyen, T. Dziomba, F. Hohls, A. Bakin, R. Stosch, C. Tegenkamp, F. J. Ahlers, and H. W. Schumacher, *ACS Applied Nano Materials* **2**, 844 (2019).
- [23] T. N. Nguyen, J. Aprojanz, M. Jäger, T. H. Nguyen, and C. Tegenkamp, *Surface Science* **686**, 45 (2019).
- [24] K. V. Emtsev, F. Speck, T. Seyller, L. Ley, and J. D. Riley, *Phys. Rev. B* **77**, 155303 (2008).
- [25] P. Giannozzi *et al.*, *Journal of Physics: Condensed Matter* **21**, 395502 (19pp) (2009).
- [26] P. Giannozzi *et al.*, *Journal of Physics: Condensed Matter* **29**, 465901 (2017).
- [27] J. Tersoff and D. R. Hamann, *Phys. Rev. B* **31**, 805 (1985).
- [28] J. D. Baran and J. A. Larsson, *Phys. Chem. Chem. Phys.* **12**, 6179 (2010).
- [29] Y. Zhang, X. Cai, X. Zhang, H. Xu, Z. Liu, and J. Jiang, *Int. J. Quantum Chem.* **107**, 952 (2007).
- [30] S. Grimme, J. Antony, S. Ehrlich, and H. Krieg, *The Journal of Chemical Physics* **132**, 154104 (2010).
- [31] K. P. Madhuri, P. Kaur, M. E. Ali, and N. S. John, *J. Phys. Chem. C* **121**, 9249 (2017).
- [32] A. Mugarza, N. Lorente, P. Ordejón, C. Krull, S. Stepanow, M.-L. Bocquet, J. Fraxedas, G. Ceballos, and P. Gambardella, *Phys. Rev. Lett.* **105**, 115702 (2010).
- [33] Y. Cai, S. Xu, X. Qiao, L. Wang, Y. Liu, T. Wang, and X. Xu, *Phys. Chem. Chem. Phys.* **17**, 23651 (2015).
- [34] S. Kera, H. Fukagawa, T. Kataoka, S. Hosoumi, H. Yamane, and N. Ueno, *Phys. Rev. B* **75**, 121305 (2007).
- [35] M. Shibuta, K. Yamamoto, K. Miyakubo, T. Yamada, and T. Munakata, *Phys. Rev. B* **81**, 115426 (2010).
- [36] R. Yamamoto, I. Yamamoto, M. Mikamori, T. Yamada, K. Miyakubo, and T. Munakata, *Surface Science* **605**, 982 (2011).
- [37] The overall total energy minimum of a free molecular layer is found for a lattice equivalent to a coverage of 1 molecule per 71 C atoms, very close to the (QF)MLG structures (1 PbPc molecule per 68 C atoms, see Table I).
- [38] W.-H. Wang, C. Gong, W. Wang, S. K. Fullerton-Shirey, A. Seabaugh, and K. Cho, *The Journal of Physical Chemistry C* **119**, 20016 (2015).
- [39] G. Wells, T. Hopf, K. Vassilevski, E. Escobedo-Cousin, N. Wright, A. Horsfall, J. Goss, A. O'Neill, and M. Hunt, *Applied Physics Letters* **105**, 193109 (2014).
- [40] D. Niesner and T. Fauster, *Journal of Physics: Condensed Matter* **26**, 393001 (2014).
- [41] M. Marks, A. Schöll, and U. Höfer, *Journal of Electron Spectroscopy and Related Phenomena* **195**, 263 (2014).